



Dynamic detection of water surface area of Ebinur Lake using multi-source satellite data (Landsat and Sentinel-1A) and its responses to changing environment



Jingzhe Wang^{a,b}, Jianli Ding^{a,b,*}, Guannan Li^c, Jing Liang^{a,b}, Danlin Yu^{e,f,*}, Tayierjiang Aishan^{b,d}, Fang Zhang^{a,b}, Jinming Yang^{a,b}, Aerzuna Abulimiti^{a,b}, Jie Liu^{a,b}

^a Key Laboratory of Smart City and Environment Modelling of Higher Education Institute, College of Resources and Environment Science, Xinjiang University, Urumqi 800046, China

^b Key Laboratory of Oasis Ecology, Xinjiang University, Urumqi 830046, China

^c Navigation College, Dalian Maritime University, Dalian 116026, China

^d Institute of Arid Ecology and Environment, Xinjiang University, Urumqi 830046, China

^e School of Sociology and Population Studies, Renmin University of China, Beijing 100872, China

^f Department of Earth and Environmental Studies, Montclair State University, Montclair, NJ 07043, USA

ARTICLE INFO

Keywords:

Ebinur Lake
Sentinel-1A
Water index
Remote sensing
Eco-environmental impact

ABSTRACT

In arid and semi-arid climatic areas, lakes are extremely essential for fragile ecological environment and regional sustainable development. Ebinur Lake is an important component of the ecological barrier of Junggar Basin, Xinjiang Uyghur Autonomous Region (XUAR), China. Due to the tremendous changes in Ebinur Lake and surrounding marshes during the last decades, Ebinur Lake becomes a representative ecological degradation region in northwestern China. The detection of the intra-annual variations of water body and its responses to changing environment are critical for regional ecological security and rehabilitation of degraded ecosystem. To extract more accurate water information using Synthetic Aperture Radar (SAR) data and further fill the gap of inter-month dynamic monitoring of Ebinur Lake, a new SAR water index (modified Sentinel 1A water index, MSWI) was proposed based on the relationship between normalized difference water index (NDWI) imageries and Sentinel 1A data. The dynamic thresholds of classification were selected using Otsu method and the results showed that the classification results were acceptable with the optimal overall accuracy of 99.94% and kappa coefficient of 0.9971, respectively. We conduct a time series analysis of surface areas of Ebinur Lake using S1A data from February 9th, 2017 to February 4th, 2018. The maximum lake surface area was 965.29 km² in April 22nd, 2017, while the minimum value was 750.37 km² in September 1st, 2017, and the mean area was 831.51 km². The seasonal variations showed the stages of “sharp rising” – “significant decreasing” – “gradual stabilizing” in the study period. The water surface area was highly correlated with inflow water volume (correlation coefficient = 0.72, $P < 0.001$). The variation of Ebinur Lake's water surface area is crucial to monitor the resulting eco-environmental impacts under the changing environmental conditions in the arid and semi-arid areas.

1. Introduction

Lakes are important surface water resources and indispensable part of the wetland environments (Ridd and Liu, 1998; Williamson et al., 2009). The evolution process of lakes and the resulting change of ecological environment are the consequence of global climate change and regional environmental variations (O'Reilly et al., 2015). The surface areas of lakes are sensitive to changing environment, specifically

human activities and climate change (Feng et al., 2012; Yang and Lu, 2014). Because of global warming, tremendous population increase and corresponding land use changes, drastic changes of lake surface areas have occurred worldwide over the past decades (George et al., 2007; Gong et al., 2013; Liao et al., 2014). Some great lakes are shrinking and even vanishing, such as the Aral Sea, Salton Sea, Dongting Lake, and Lop Nur (Birkett and Mason, 1995; LeBlanc and Kuivila, 2008; Shao et al., 2012; Singh et al., 2012). The dynamics of lake water surface

* Corresponding authors.

E-mail addresses: watarid@xju.edu.cn (J. Ding), yud@mail.montclair.edu (D. Yu).

areas are essential for understanding how lakes are responding to the changing environment (Holmgren et al., 2006; Stanev et al., 2004). Therefore, identifying and mapping the lake water surface areas, and detecting their changes have attracted considerable attention in recent years.

With the capability of wide view field, high efficiency, low cost, real-time information acquisition and periodic surface coverage, satellite remote sensing technology has been widely accepted as an efficient and appropriate means for extracting and monitoring the change of water bodies across various spatial-temporal scales (Feng et al., 2011; Haas et al., 2011; Ma et al., 2010). Satellite data collected from optical remote sensors, such as moderate resolution imaging spectroradiometer (MODIS), Landsat series, HuanJing satellite constellation-1 (HJ-1) and GaoFen-1 (GF-1) have been applied to the change detection of lake water surface areas at different spatial resolutions (Feng et al., 2012; Liao et al., 2014; Sharma et al., 2015). Because of strong spectral absorption in the near-infrared (NIR) and shortwave infrared (SWIR) spectra of water body on satellite images, various spectral indexes, such as normalized difference water index (NDWI), modified normalized difference water index (MNDWI), enhanced water index (EWI), revised normalized difference water index (RNDWI) and other water body detection indexes were developed (Lacaux et al., 2007; Lillesand et al., 1994; McFeeters, 1996; Wang et al., 2015; Xu, 2006). In recent decades, many researchers have studied the dramatic changes in lake water surface area. Liao et al. (2014) applied Landsat series and China's HJ-1 satellite images for the global water surface cover extraction and mapping (Years 2000 and 2010) and developed the first set of high-resolution (30 m) global land water data product for the two periods.

The spatial and temporal resolutions of optical satellite imagery are continuously improving. However, the water index value is based on optical remote sensing data, which are easily influenced by clouds. It is difficult for optical remote sensing satellites to provide enough data for periodic surface observation of water surface areas (Alesheikh et al., 2007; Zeng et al., 2017). Synthetic Aperture Radar (SAR), an active microwave imaging sensor, could operate in all-time and all-weather conditions and meet the demand of water body dynamic monitoring (Horritt et al., 2001; Mason et al., 2012). By evaluating the intensity, polarimetric scattering, interferometric coherence, and spatial texture of Phased Array type L-band SAR (PALSAR) imagery, Jin et al. (2014) extracted the water body in the Onondaga County (Central New York State, USA) with an acceptable overall accuracy of 91%. Brisco et al. (2009) applied RADARSAT-1 imagery and semi-automated extraction tools for the annual and seasonal change of inland water bodies in northern Canada. Sentinel-1A satellite image, an open access data source, possesses relatively fine resolution (typically 20 m), a 12-day return cycle, as well as wide swath of 250 km (Torres et al., 2012). Sentinel-1A data could provide novel opportunities for monitoring lake water surface area changes. Zeng et al. (2017) detected the recent water surface area changes of Poyang Lake with the threshold method during the observation period (October 2014 to March 2016) using the Sentinel-1A data, which demonstrated its potential in dynamic water body observation. In addition, a novel Sentinel-1A water index (SWI) has been built and applied to the dynamic water area change detection of the biggest freshwater lake in China (Poyang Lake), demonstrating its validity in detecting water surface area information in humid climatic areas (Tian et al., 2017).

In arid and semi-arid climatic areas, lakes are extremely essential for the fragile ecological environment and regional sustainable development (Bai et al., 2011). Ebinur Lake is a representative ecological degradation region which located in the Xinjiang Uyghur Autonomous Region (XUAR) of northwestern China. There are tremendous changes in Ebinur Lake and surrounding marshes during the last decades (Wang et al., 2017a). Ebinur Lake and the adjacent marshes are essential for threatened local biodiversity, which have been considered as the effective indicators for the watershed ecosystem health (Liu et al., 2011). Recently, preservation of Ebinur Lake has attracted enormous

governmental concerns. To protect the critical ecosystems and oasis ecology of Junggar Basin, Ebinur Lake Wetland National Nature Reserve has been listed in the National Nature Reserve List of China (Wang et al., 2017a). The lake's water surface area has been examined with satellite imagery previously, but only during specified periods in summer or autumn (Jing et al., 2018; Ma et al., 2014; Ma et al., 2007; Zhang et al., 2014). Furthermore, its annual and intra-annual variations are rarely documented in detail, and the effect of streamflow and other natural factors on Ebinur Lake surface area have not been sufficiently analyzed.

This study attempts to fill the gap of inter-month dynamic monitoring of Ebinur Lake's water surface area and the driving forces for its changes. The main objectives of this study are as follows: (1) to propose a new SAR water index (modified Sentinel 1A water index, MSWI) and validate its feasibility in the study area; (2) to monitor the inter-annual and intra-annual water surface area changes of Ebinur Lake; and (3) to examine the driving forces of the dynamic variations.

2. Study area

Ebinur Lake, the largest saltwater lake in XUAR, is located in the southwest of the Junggar Basin, between 44°43' to 45°12' N and 82°35' to 83°40' E (Fig. 1). The study area has the lowest elevation in the Junggar Basin (189 m). It is also the center of the Ebinur Lake Watershed (Liu et al., 2011). The lake area has a typical continental arid climate, characterized by dramatic annual temperature change, scarce precipitation (89.80–169.70 mm), and strong potential evaporation (1569–3421 mm, $6.8 \times 10^8 \text{ m}^3/\text{yr}$) (Ma et al., 2014). Another characteristic in the Ebinur Lake region is the constant strong winds. On average, winds with speeds > 8 m/s occur on 164 days per year, reaching a maximum of 185 days per year (Wang et al., 2018a). The lake is a typical terminal lake in arid and semi-arid areas, which receives chemical substances and sediments carried by runoff (surface and subsurface) and atmospheric deposition (Wang et al., 2017a). The emerged lake bottom during the low water level serves as the habitat for a wide range of wild birds, making Ebinur Lake region one of the most important migration channels for birds in central and northern Asia (He et al., 2015).

Ebinur Lake and the adjacent wetlands are also regarded as the core areas of Oasis–Desert System in the northern slopes of the Tianshan Mountains (Ge et al., 2016). Since the early 1950s, the surface area of Ebinur lake has shrunk visibly. This is mainly because of the constant climatic fluctuation and increasing human influence such as increasing population densities, drastic oasis expansion, rapid agricultural development and consequently reduced surface runoff (Liu et al., 2015). At present, Ebinur Lake is mainly charged by ground water and surface runoff from the Jinghe River and Bortala River. The shrink of Ebinur Lake has exposed broad hard salt crusts and saline desert. The bare dry lakebed comprises abundant loose saline sediments and has been recognized as one of the main sources of dust and salt dust in Central Asia, which might cause severe ecological degradation to local fragile environment (Ge et al., 2016).

3. Materials and methodology

3.1. Remote sensing imagery and pre-processing

Landsat-8 OLI (Operational Land Imager) and Sentinel-1A (S1A) data were used in this study. These images were obtained from the United States Geological Survey (<http://glovis.usgs.gov/>) and European Space Agency's Copernicus Open Access Hub (<https://scihub.copernicus.eu/>). The captured remote sensing data are raw Level-1 images without any pretreatment.

Sentinel-1 was launched on April 3rd, 2014. It is equipped with a C-band (5.405 GHz) SAR instrument and offers a standard revisiting period cycle of 12 days (Geudtner et al., 2014). Generally, S1A SAR

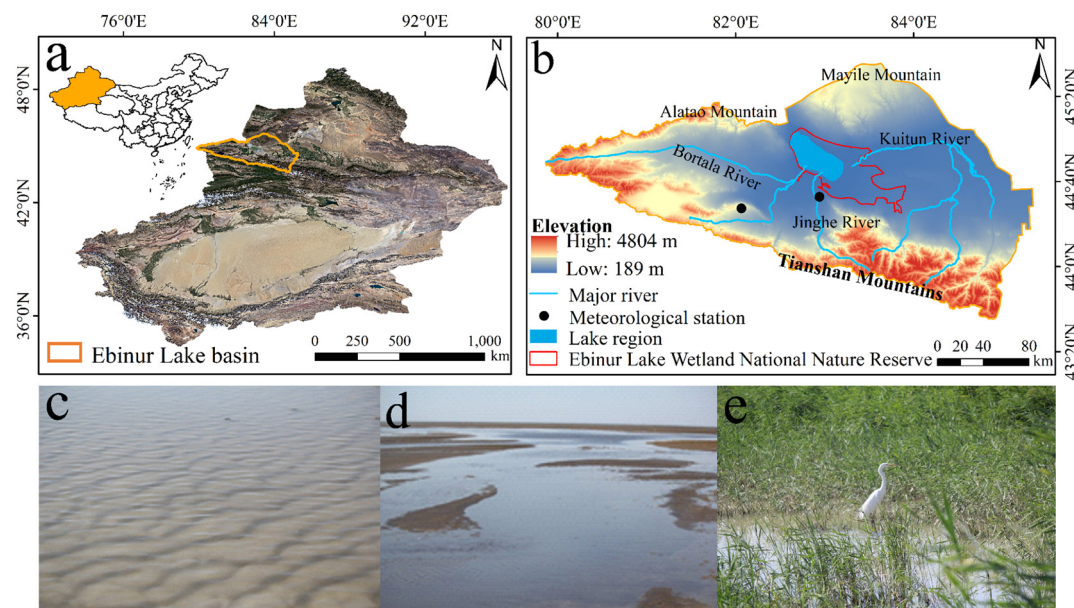


Fig. 1. Location map of the study area and typical landscape photograph. (a: Location of Xinjiang Uyghur Autonomous Region, b: Ebinur Lake basin, c: Water body, d: Lake bed, and e: Lake-side wetland).

data can be obtained in different acquisition modes including Stripmap mode (SM), Interferometric Wide Swath mode (IW), Extra-wide Swath mode (EW), and Wave mode (WM) (Plank, 2014). In this study, we focus on the standard Level-1 (ground range detected, GRD) data product in IW mode with dual-polarization (VV/VH). This satellite imagery has a wide swath of 250 km, pixel spacing of 10 m, and the spatial resolution of 5 m and 20 m in range and azimuth directions, respectively. The detailed description of S1A data is available in other studies (Malenovský et al., 2012; Torres et al., 2012) and will not be repeated here. In this study, 31 S1A satellite scenes were selected from February 9th, 2017 to February 4th, 2018. The reason why we choose the images in this specific period is, the surface area of Ebinur lake in 2017 has reached an all-time high based on the environmental report of XUAR (Wang et al., 2018a). We applied the SNAP (Sentinel Application Platform) toolbox (<http://step.esa.int/main/toolboxes/snap/>) to pre-treat the S1A data by ourselves. The main steps of preprocessing are described as follows:

- (1) Apply orbit files (POD, Precise Orbit Ephemerides, <https://qc.sentinel1.eo.esa.int/>).
- (2) Conduct radiometric calibration (to output sigma 0 bands).
- (3) Execute Range-Doppler terrain correction (SRTM DEM with the spatial resolution of 30 m).
- (4) Acquire backscattering coefficient (in dB scale).
- (5) Remove speckle noises. Considering the filtering results and processing efficiency, median filter in the window size of 5×5 px was used (Eweys et al., 2017; Passaro et al., 2018; Tian et al., 2017).

Landsat-8, an American Earth Observation satellite, was launched on February 11th, 2013. It carries two push-broom instruments, namely, the OLI and Thermal Infrared Sensor (TIRS). The Level-1 data products of Landsat-8 OLI contain seven spectral bands with a spatial resolution of 30 m (Roy et al., 2014). Two simultaneous cloud-free Landsat-8 OLI scenes captured on June 9th, and July 27th, 2017 were used for the construction and capability validation of MSWI and dynamic detections of water body. In this study, each raw Landsat image has undergone radiometric calibration and atmospheric correction to convert digital number values into surface reflectance for spectral indices calculation (Deng et al., 2017). The ENVI® software version 5.1 (Exelis Visual Information Solutions, Boulder, CO, USA) and ArcGIS®

software version 10.1 (ESRI, Redlands, CA, USA) were used to preprocess the OLI images. The processing consists three steps:

- (1) Radiance calibration (to output Top Of Atmosphere (TOA) reflectance).
- (2) Fast Line-of-sight Atmospheric Analysis of Hypercubes (FLAASH) atmospheric correction (to output surface reflectance).
- (3) Geometric correction (< 0.5 pixels).

In addition, the remote sensing dataset used for this study were re-projected to the uniform coordinate reference system (WGS 84 UTM Zone 44 N). Then, stacked pixels were aggregated to match the spatial resolution of Landsat OLI imagery (30 m) using the nearest-neighbor resampling method. The operation of resampling also reduces the size of the dataset and further improve the execution efficiency (Li et al., 2017; Tian et al., 2018). The temporal distribution of the utilized S1A images and Landsat-8 OLI images during the study period is illustrated in Fig. 2. For the analysis of the inter-annual water surface area changes of Ebinur Lake from 1990 to 2016, we collected the historical Landsat data and NASA data from <http://earthdata.nasa.gov/data/near-real-time> data and <https://earthdata.nasa.gov/labs/worldview/>.

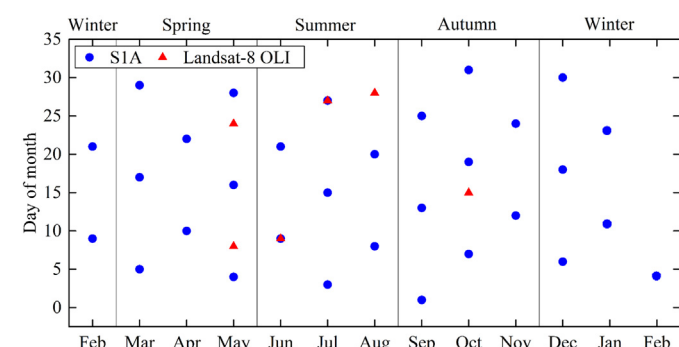


Fig. 2. Temporal distribution (day of month) of satellite images adopted in the present study.

Table 1
Information of inflow runoff stations used in this study.

River	Inflow runoff station	Latitude/°N	Longitude/°E	Elevation/m
Bortala River	Wuzhiqu	44°53'28"N	82°39'52"E	194
	Zongpai	44°51'57"N	82°40'48"E	193
	Major bridgeI	44°45'59"N	82°39'10"E	238
Jinghe River	Major bridgeII	44°41'37"N	82°49'53"E	235

3.2. Hydro-meteorological datasets

The daily air temperature and precipitation data in Ebinur Lake region were collected from two meteorological stations (the Jinghe and Bole station) in the China Meteorological Data Service Center (<http://data.cma.cn/en>) for the period 1990–2016. The surface area data of Ebinur Lake and the runoff data of Bortala River and Jinghe River (mountain-pass runoff and inflow runoff) during the entire period were acquired from the Hydrological Bureau of XUAR, China. The detailed geographical positions of these inflow runoff stations are shown in Table 1.

3.3. Water body extraction

The optical water spectral indexes (NDWI and MNDWI) could maximize spectral features of water and enhance the contrast between water and land area (Xu, 2006). Compared to the NDWI, MNDWI concerns more about the spectral information of urban building in the SWIR band. For instance, in Tian et al. (2017)'s study of Poyang Lake,

which is located in the northern Jiangxi Province, China, and surrounded by urban and dense built-up areas (the Poyang Lake urban agglomeration), MNDWI is regarded as an effective method for urban water surface extraction. Based on the negative relationship between S1A and MNDWI scenes, Tian et al. (2017) performed the stepwise regression analysis between S1A data (VH, VV, and other polarization-derived parameters) and MNDWI to develop the SWI. Consequently, SWI is a MNDWI-like index, and the fitted equation is statistically significant with a *p*-value < 0.01. The dynamics of Poyang Lake were monitored based on this newly developed water index and S1A data.

Different than the principles of using optical water spectral indexes (e.g., NDWI and MNDWI) to measure water bodies, the extraction of water body using SAR imagery is based on the intensity difference of radar pulses of water and non-water areas (Silveira and Heleno, 2009). Generally, waterbodies are considered the smooth and homogenous surfaces, generate weaker echo intensity. The non-water areas with different roughness commonly produce stronger return of radar pulses (Kyriou and Nikolopoulos, 2015). Accordingly, the SAR imaging features of waterbodies and non-water areas are bright and dark, separately.

Since the Sentinel 1A water index (SWI) is a MNDWI-based index, it has similar characteristics as MNDWI. However, Zhang et al. (2014) compared the accuracy of MNDWI and NDWI for water extraction using Landsat images in Ebinur Lake and found that MNDWI could result in misclassification of water and surrounding dry lakebed, because it tends to minimize the effect of dry lakebed and mountain shadow. This suggests that NDWI might be a more appropriate spectral index under the lake area environments in arid regions. Considering the difference,

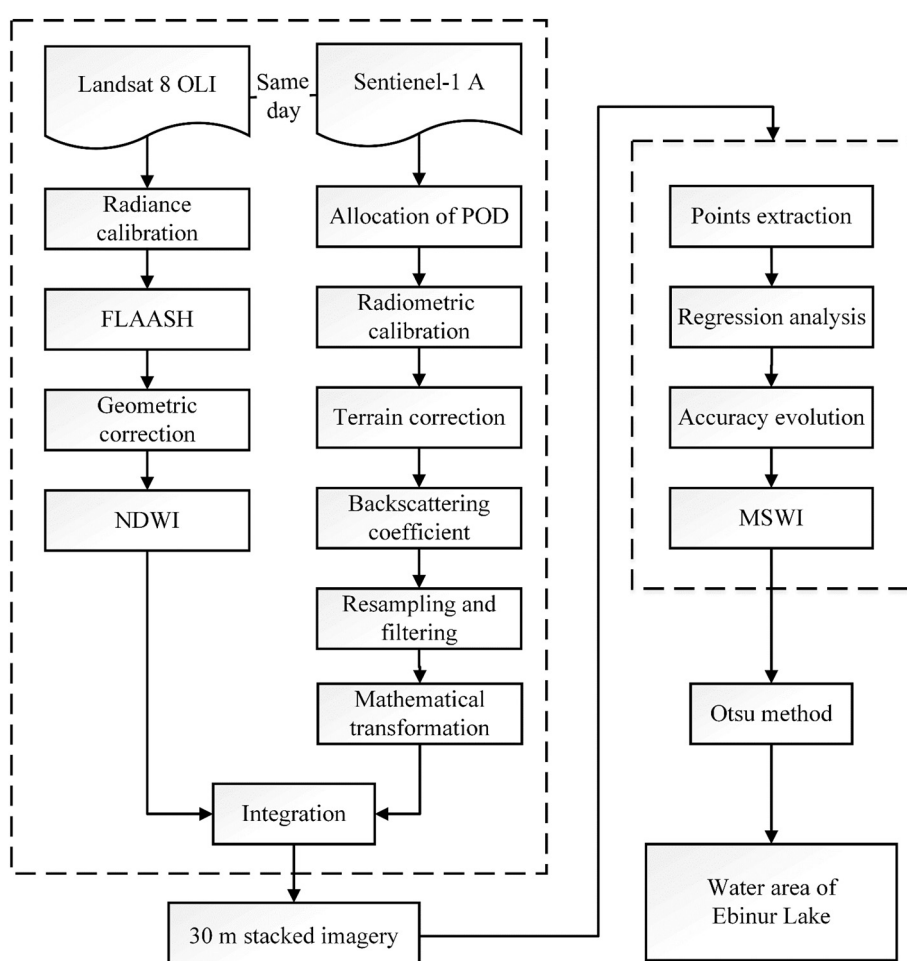


Fig. 3. Schematic diagram of overall workflow.

the capability of SWI to measure water bodies might suffer from such potential limitations in this study. Hence, this study attempts to modify it based on NDWI and propose a modified Sentinel 1A water index (MSWI) for dynamic detections of water surface area in the study region.

The formulations of NDWI, MNDWI and SWI are described as follows:

$$\text{NDWI} = (\text{Green} - \text{NIR}) / (\text{Green} + \text{NIR}) \quad (1)$$

$$\text{MNDWI} = (\text{Green} - \text{SWIR}) / (\text{Green} + \text{SWIR}) \quad (2)$$

$$\text{SWI} = 0.1747 \times \text{VV} + 0.0082 \times \text{VV} \times \text{VH} + 0.0023 \times \text{VV}^2 - 0.0015 \times \text{VH}^2 + 0.1904 \quad (3)$$

where Green, NIR and SWIR represent the reflectance of Green band (band3, 525–600 nm), NIR band (band5, 845–885 nm) and SWIR band (band6, 1560–1660 nm) in the OLI imagery, respectively; VH and VV represent the backscattering coefficient in VH polarization and VV polarization in S1A data, respectively.

The Otsu method (maximum between-cluster variance method) is a well-accepted algorithm for segmenting index images for land cover object detection because of its relative accuracy and high efficiency (Dalmonte et al., 2014; Otsu, 1979; Rosser et al., 2017). This method was used for the selection of threshold in each image to distinguish lake water area from the background in this study. The threshold of each satellite image was calculated in the Interactive Data Language, IDL® software version 8.3 (Exelis Visual Information Solutions, Boulder, CO, USA).

The schematic diagram of the overall workflow is illustrated in Fig. 3.

3.4. Accuracy evaluation

The water area extracted from Landsat-8 OLI using visual interpretation was regarded as the ground-truth lake water area to examine the classification accuracy of S1A (Deng et al., 2017; Tian et al., 2017). The ground-truth water areas from OLI (two OLI scenes acquired on July 7th and September 9th, 2017) were selected to assess the accuracy of the MSWI category using the confusion matrix method. Finally, the parameters of Kappa coefficient, means producer's accuracy, means user's accuracy, and means overall accuracy were used for the quantity accuracy assessment (Haas et al., 2011).

Four indices are used to evaluate the fitting performance of the newly developed MSWI in this study: the determinant coefficients (R^2), root mean square errors of calibration (RMSE), root mean square errors of prediction (RMAPE), and mean absolute error (MAE). Their detailed mathematical expressions have been given in Bennett et al. (2013) and Chai and Draxler (2014), and will not be repeated here. In general, better fitting performance is represented with high values of R^2 but low values of RMSE, RMAPE and MAE.

3.5. Dynamic degree of the lake water surface area

Dynamic degree (K) of the lake water surface area represents the variation ratio of water body in different observation periods. This index quantifies the developing trend and rate of shrinkage and expansion of a specific water body (Li et al., 2009). It was calculated as follows:

$$K = \frac{U_b - U_a}{U_a} \times \frac{1}{T} \times 100\% \quad (4)$$

where K represents the dynamic degree of the lake surface area; U_a and U_b represent the surface areas of the lake at the beginning and end of the study period, respectively; and T represents the time step interval (Liu et al., 2003).

3.6. Mann-Kendall trend detection test

The nonparametric Mann-Kendall method (M-K) recommended by the World Meteorological Organization (WMO) (Kendall, 1975; Mann, 1945) was used to analyze change trends for hydrological data. The detailed mathematical expressions have been given in (Ahmad et al., 2015; Kisi and Ay, 2014). In this study, the parameters of the M-K test such as coefficient of variation (C.V.), standardized score (Z), and Sen slope estimator (E_o) are calculated.

4. Results

4.1. The construction of MSWI

Polarization information is the striking characteristics of SAR satellite images. In essence, the information derived from SAR data is the reflected radar wave of the physical objects. The image is mainly formed by backscattering properties. The echo signal differs according to different polarization modes. The physical mechanism of co-polarization amplitudes (i.e., HH and VV) is similar to the mirror reflections. However, the cross-polarization amplitudes (i.e., HV and VH) are commonly affected by the heterogeneous surface roughness, causing weaker returned SAR echo response (Geudtner et al., 2014).

Many SAR-based studies employed either histogram thresholding methods and/or classification approaches to map water surface (Stephanie et al., 2014; Zeng et al., 2017). The mathematical transformations of dual-polarized data are efficient in terms of enhancing the separability between different classes (Amani et al., 2017; Mahdavi et al., 2017). For SAR index, most studies have reported that the ratio features (e.g., VV/VH and HH/VH) could generate better performance (Brisco et al., 2011; Veloso et al., 2017; Zhuang et al., 2018). In this study, eight S1A-based parameters (VV, VH, VV/VH, VH/VV, VH-VV, VV × VH, VV², and VH²) were considered for the construction of MSWI. Box plots of these polarization-derived parameters by water and non-water classes are presented in Fig. 4, which demonstrate that the parameters of VV × VH, VV², and VH² enhance the class separability between water and non-water classes. These approaches distinguish well between different pixels, since they can extract and summarize the important signal portions that help the classification task between water and non-water classes. However, the ratio index did not enhance the separability between different classes as expected, which could be attributed to the relative homogeneous underlying surface in Ebinur Lake region.

For better classification results, six additional parameters (i.e., VV, VH, VH-VV, VV × VH, VV², and VH²) were derived from the results of the band operation on S1A imagery. The NDWI imagery was obtained by means of Eq. (1). Then, the pretreated S1A data with multiple attributes were stacked with NDWI, which means that every cell has seven (stacked) attributes. A total of 872 random points were generated using the "Create Random Points" tool in ArcGIS 10.1. The points are distributed evenly in the study area, covering water body, wetland, forest-grassland, cropland, saline land, and bare land. To reduce the impact of the changing of lake water surface area in different acquisition time, both optical and SAR remote sensing imageries were collected on the same date (July 25th, 2017). The stepwise regression analysis approach was applied to generate MSWI. In the regression analysis, NDWI was defined as the response variable, while the S1A-derived parameters were the independent variables.

Based on the correlation between NDWI imagery and S1A data (including polarized bands and transformations), the fitting of MSWI was carried out using regression method. In the fitted model of MSWI, variables of VH, VH-VV, VV × VH, VV² and VH² were selected. The resulting formulations of MSWI is described as follows:

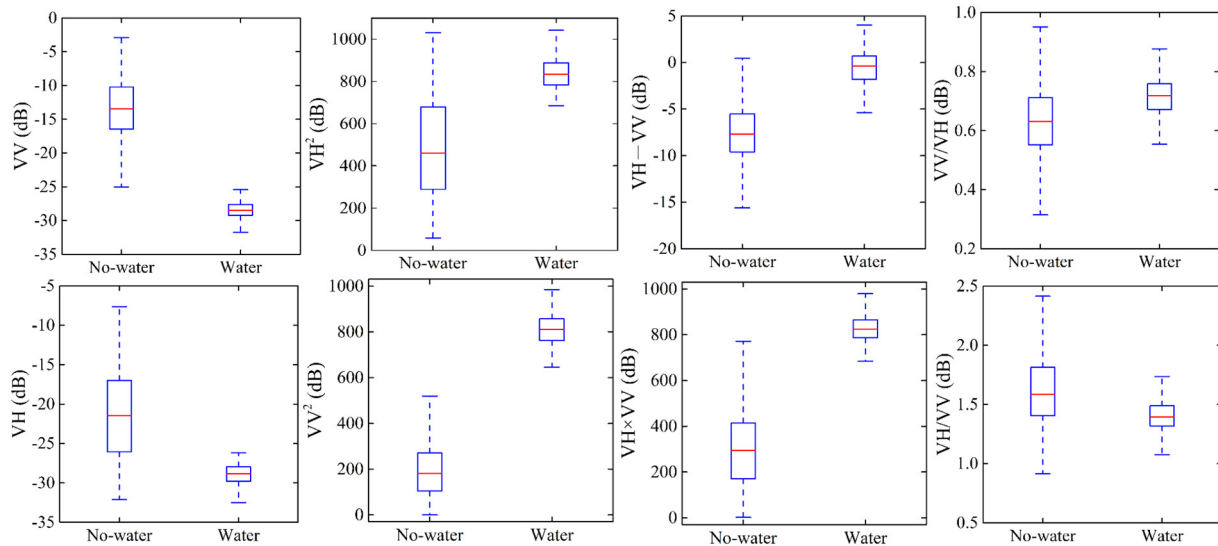


Fig. 4. Box plot of eight S1A-based parameters (VV, VH, VV/VH, VH/VV, VH-VV, VV × VH, VV², and VH²) in water and non-water classes. (Red bar is the median value and blue box shows the first and third quantile). (For interpretation of the references to color in this figure legend, the reader is referred to the web version of this article.)

$$\text{MSWI} = 0.00045 \times \text{VH} - 0.027687 \times (\text{VH} - \text{VV}) - 0.00429 \times \text{VV} \times \text{VH} + 0.00489 \times \text{VV}^2 - 0.00147 \times \text{VH}^2 - 0.92412 \quad (5)$$

where VH and VV represent the backscattering coefficient in VH polarization and VV polarization in S1A data, respectively.

The accuracy evaluation and statistical tests were conducted to assess the reliability of the index. An F-test's *p*-value of < 0.001 indicated that the regression equation was statistically significant. The regression equation was reliable with the values of $R^2 = 0.91$, RMSE = 0.18, RMAPE = 0.05, and MAE = 0.14. To further verify the performance of MSWI, it was checked in another period (June 9th, 2017). The testing results are acceptable based on the accuracy indices (Table 2).

4.2. Detection of lake water surface area

The accurate threshold is critical to segment water bodies from surface features information. The strategy for the threshold selection is derived from the histogram frequency of the specific remote sensing imagery. A fixed threshold value might result in omissions and/or misclassifications, when it was applied in other scenes. Thereby, we applied Otsu method to identify the ideal threshold for each MSWI scene during the entire period. The threshold had a narrow range of 0.19–0.39 with a mean value 0.31 (Fig. 5). Since the MSWI is a NDWI-based index, it has similar characteristics as NDWI. Thresholds of MSWI obtained in the current study agree well with published studies using NDWI in the same study area (Zhang et al., 2014; Zhang et al., 2015). Therefore, the selected thresholds are reasonable and feasible and could be used for water body detection. For each scene, a pixel is classified as water if its MSWI value is more than the corresponding threshold value. The dynamic changes of Ebinur Lake water surface area are illustrated in Figs. 6 and 7. During this period, the maximum lake surface area was 965.29 km² (April 22nd, 2017), while the minimum value was 750.37 km² (September 1st, 2017). The mean area was 831.51 km². Only five cloud-free Landsat-8 OLI scenes captured on May 8th, May

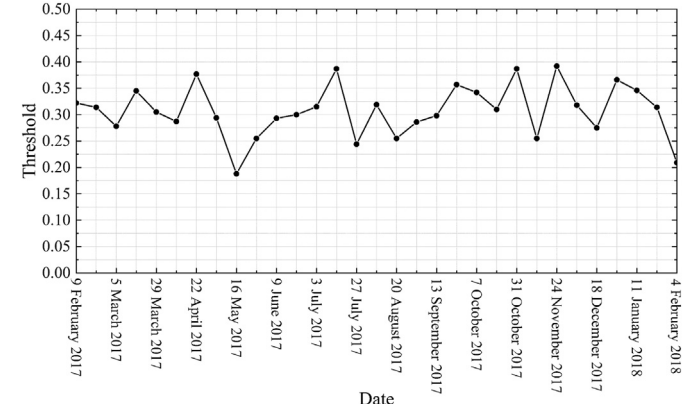


Fig. 5. The threshold for each MSWI scene determined by Otsu method.

24th, June 9th, July 27th, and August 28th, 2017 were used. The comparison between indexes of NDWI and MSWI based on Landsat-8 OLI and S1A data is shown in Fig. 7. Our analysis detects clearly substantial dynamic variations of Ebinur Lake water surface area, which were not reported previously.

To quantify the developing trend and change rate of Ebinur Lake, the shrinkage and expansion of water bodies were statistically analyzed with a time step interval of 12 days. During the period from March 29th to April 10th, 2017, the lake area expanded by 84.36 km² with a maximum dynamic degree of 9.78%. The sharpest shrinkage of water body was observed from July 15th to July 27th, 2017 (-78.51 km²). The variations from Summer-Autumn months (from May to November) were most dramatical. The monthly minimum waterbody area of the Autumn season is < 77.74% of that in April. There were seven changes > 5%, with the mean changing rate of 4.7%. In the present study, the average water surface area in April was 937.23 km² but shrank to 782.44 km² (the smallest) in September. The seasonal variations showed the stages of “sharp rising” – “significant decreasing” – “gradual stabilizing” in the study period. The change of the lake's water surface area was mainly in the northwestern part of Ebinur Lake. This is because the river estuaries are located in the southeastern area. In addition, in the northwestern part of the Lake, the effects of evaporation and infiltration during the motion process of lake water as well as the sub-aqueous terrain are far more active than elsewhere (Liu et al.,

Table 2
The accuracy evaluation and statistical tests results of MSWI.

Date	Pixels	R ²	RMSE	RMAPE	MAE
July 27th, 2017	872	0.91	0.18	0.05	0.14
June 9th, 2017	312	0.93	0.19	0.06	0.15

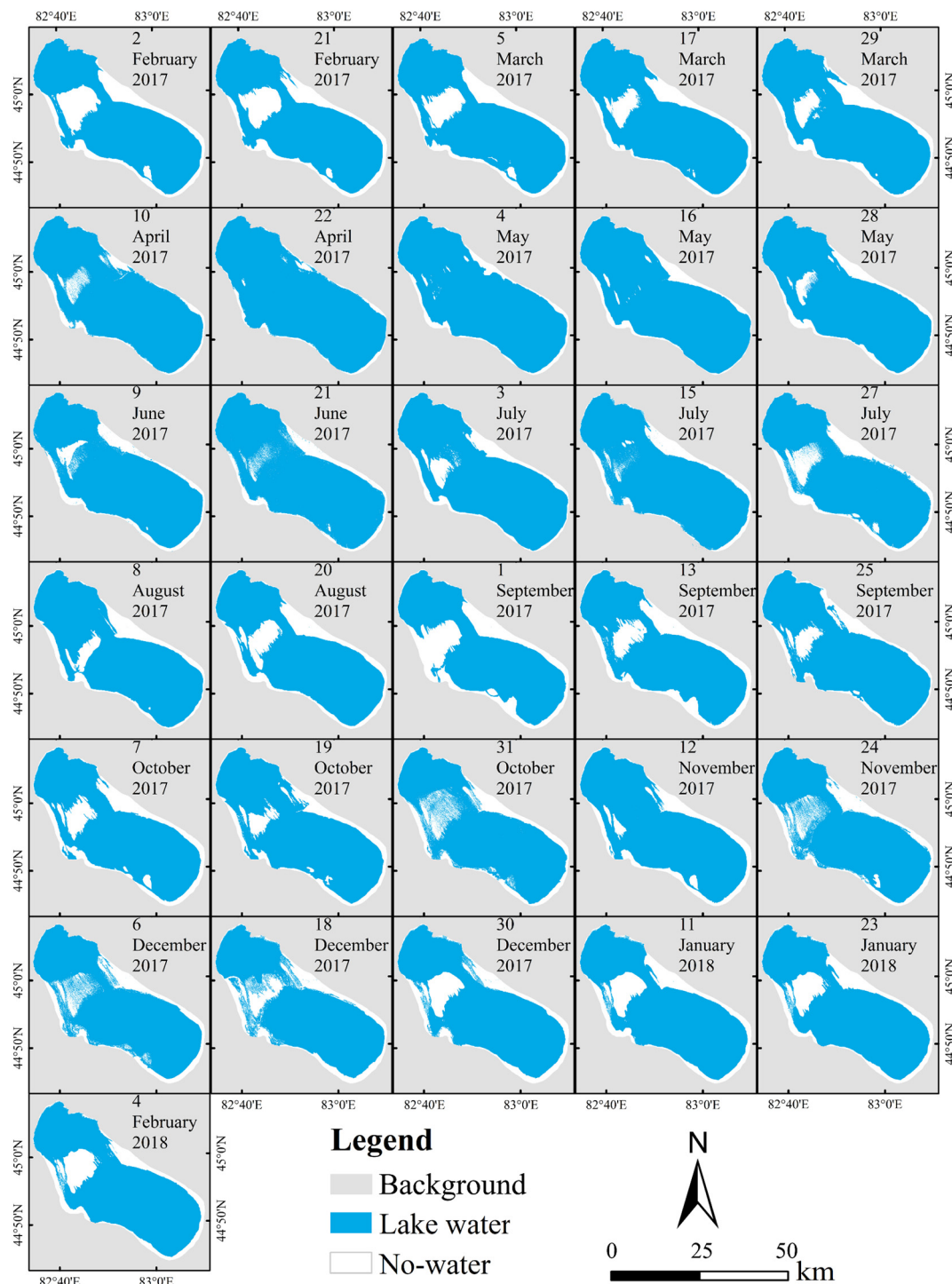


Fig. 6. The 12-day interval spatial-temporal distributions derived from Sentinel 1A data using MSWI for Ebinur Lake from February 9th, 2017 to February 4th, 2018.

2002). In general, the maximum surface area of the lake in the northern XUAR is in Spring and the minimum value in Summer. The results of the present study agree well with existing research (Li et al., 2015; Ma et al., 2007).

4.3. Accuracy verification

To evaluate the classification accuracy of MSWI, the methods of Minimum Distance Classification (MDC) and NDWI based on Landsat-8 OLI were applied for the water body detection. The results are reported in Table 3 and Fig. 8. Compared to the results of NDWI and MDC, MSWI

yields better overall accuracy in the study area. On July 27th, 2017, the producer's accuracy and user's accuracy of water class are 98.83% and 99.58%, respectively. As for the kappa coefficient, the result in June 9th, 2017 is better (0.9971). The results suggest that the MSWI can be used for the dynamic detections of water surface area in our study with ideal accuracy.

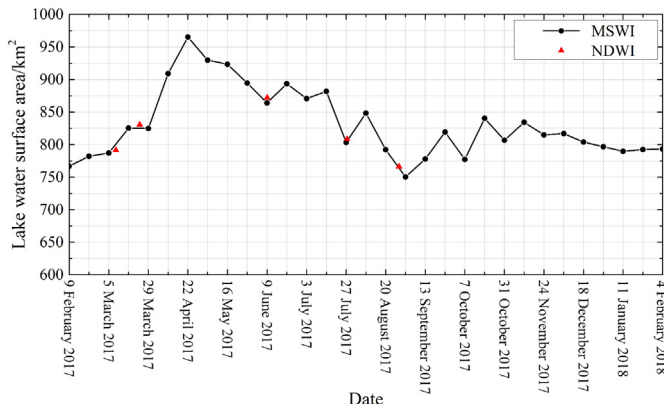


Fig. 7. The extracted surface of Ebinur Lake based on different methods (MSWI versus NDWI) from February 9th, 2017 to February 4th, 2018 with a time step interval of 12 days.

5. Discussions

5.1. Driving forces of the dynamic variations

The changes in the lake water surface areas are important indicators for different environmental conditions at multiple time scales (Bai et al., 2011). The inter-annual variations of lakes' water surface areas often reflect the impacts of changing temperature and precipitation, which laid the foundation for analyzing the mechanism of regional lake water surface area change (Beeton, 2002; Li et al., 2015). On the other hand, the research on seasonal variations of lake water surface areas is conducted with the synthetic effects of regional precipitation, evaporation, groundwater and other related factors, which are important to understand local hydrological cycle (Ma et al., 2010).

To further quantify the driving forces for the variations of the lake's water surface area in the study area, analyses were conducted with the regional hydro-meteorological datasets. The results are presented in Fig. 9. In general, the change of water surface area follows closely the inflow volume change. A few anomalies are mainly attributable to the effects of transformation between surface and subsurface streams (Su et al., 2016; Wang et al., 2018b). During the observation period, the most obvious fluctuation (from 482.03 km² to 824.47 km²) was in the period from 2001 to 2009. The annual precipitation and runoff in the study area were gradually increasing, which led to the dramatical fluctuation in the surface area of the lake (Figs. 10 and 11).

We also analyzed the general trends of the runoff in Jinghe River and Bortala River (Table 4). The runoff in Jinghe River station was gradually increasing, while decreasing slightly in the Bortala River. The correlation coefficients between the water surface area of Ebinur Lake

and the hydro-meteorological data were further calculated as shown in Fig. 12. The correlation between water surface area and inflow water volume was the highest (r -value = 0.72, $P < 0.001$), indicating that variations in the water surface area of Ebinur Lake are significantly correlated with the change of inflow water at the yearly scale. The annual mountain-pass runoff and precipitation in Jinghe and Bortala River did show good relevance. The mountain-pass runoff is not highly correlated with the water surface area (r -value = 0.31 in Jinghe River). One reason for this discrepancy is because of the effects of human activities (irrigation and construction of hydrological projects) in this region, which often results in out-sync between runoff and water surface area extension (Bao et al., 2006; Li et al., 2015). Another reason is the special runoff characteristics of Bortala River. The runoff is richer in Winter months than in Summer months. In addition, the groundwater might impede the inflow water from rivers to the lake (Su et al., 2016; Zhang et al., 2014).

5.2. Uncertainty analysis

Affected by geological conditions, hydrographic geology, and other factors, the average depth of Ebinur lake is shallow (approximately 1.40 m). Furthermore, the Alataw Pass (near the Alatao Mountain) is an entrance for strong prevailing wind in this region (Fig. 1). Under such conditions, the water surface area of Ebinur Lake is extremely sensitive to the wind (direction and speed). The northwestern part of Ebinur Lake is closer to the Alataw Pass, together with the scarce vegetation cover and frequent strong wind, the surrounding flat open lake-side regions are strongly affected by overflow lake water and stormy waves, both are caused by the prevailing northwestern wind. In addition, the stormy waves can take the highly mineralized lake water to the nearby shores, which promotes the formation and development of wetland (Liu et al., 2002). Affected by these factors, the actual water surface of Ebinur Lake can change visibly within a day. Although simultaneous remote sensing imageries were used for the extraction of water surface, it is worth noting that there will always be temporal mismatch between different remote sensing data.

The edges of the water body are the main areas where misclassifications occurred because these landscapes are relative complex. The zones of the misclassification of water area mainly appeared as a dark color-region in true-color Landsat-8 scene (Fig. 13). There are shoal water or submerged land in these regions, and their spectral characteristics are similar to those of the normal water (Fig. 14). Hence, these pixels might be categorized as water body by mistake.

Inherent speckle noises in SAR imagery usually complicate visual interpretation and make it difficult to extract useful information (Dong et al., 2018). In this study, the median filter gives us the best filtering results and processing efficiency, especially for the speckle noises. The 5×5 pixels-window is appropriate for a homogeneous area because it

Table 3
Confusion matrix for the water extraction using different data acquired on July 7th and September 9th 2017.

Date	Method	Class	Commission (%)	Omission (%)	P.A. (%)	U.A. (%)	O.A. (%)	Kappa Coefficient
July 27th, 2017	MDC	Water	1.30	1.75	98.25	98.70	99.38	0.9808
		Non-water	0.45	0.33	99.67	99.55		
	NDWI	Water	6.46	1.16	98.84	93.54	99.17	0.9619
		Non-water	0.04	0.95	99.05	99.96		
	MSWI	Water	0.42	1.17	98.83	99.58	99.69	0.9901
		Non-water	0.28	0.10	99.90	99.72		
June 9th, 2017	MDC	Water	8.29	3.28	96.72	91.71	98.19	0.9453
		Non-water	0.49	2.27	97.73	99.51		
	NDWI	Water	1.85	3.53	96.47	98.15	96.71	0.9004
		Non-water	0.90	3.24	96.76	99.10		
	MSWI	Water	0.31	0.21	99.79	99.69	99.94	0.9971
		Non-water	0.03	0.04	99.96	99.97		

Note: P.A. means producer's accuracy; U.A. means user's accuracy; and O.A. means overall accuracy.

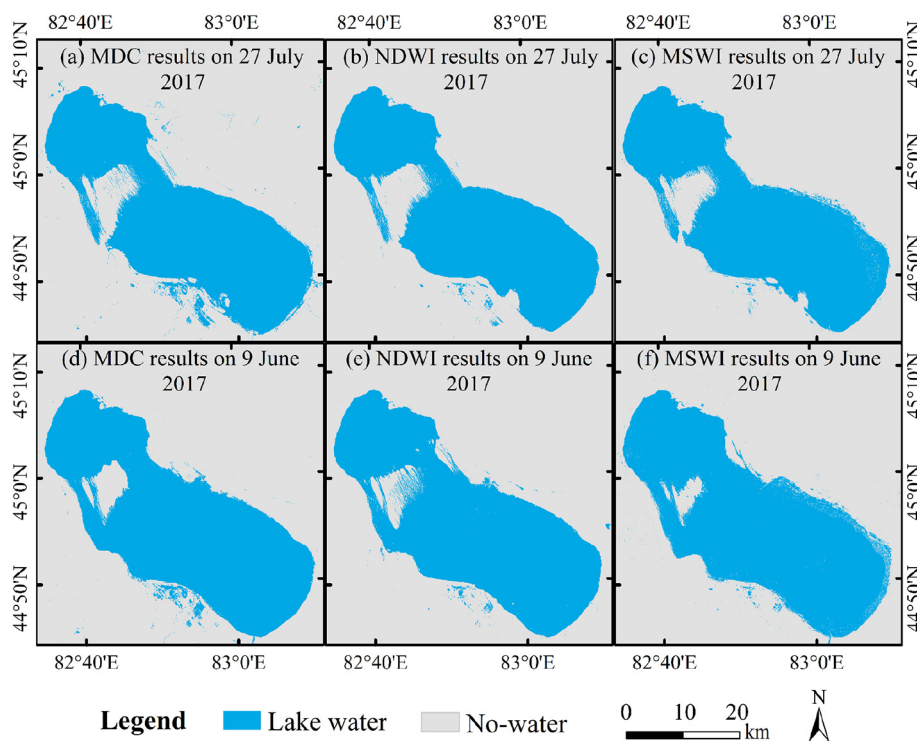


Fig. 8. Classification accuracy comparison between Landsat-8 OLI image and water surface information map NDWI and MSWI.

is beneficial to significantly restrain the negative influence of speckle noise, thereby accurately describing the change occurred in SAR images (Eweys et al., 2017; Tian et al., 2018; Zhuang et al., 2018). In addition, it was reported that the multi-temporal filters and non-local speckle filters with adaptive window size could also potentially reduce the speckle-noise while achieving maximum retention of valid information of the data (Zhao et al., 2015).

Although both the proposed Sentinel 1A water indexes are easily calculated and provide high accuracy, it is still necessary to realize there are uncertainties when applying them. The main issue of these empirically produced statistical indexes is their limited transferability to different sites. In fact, the proposed SWI and MSWI are obtained using specific data (data from Poyang Lake or Ebinur Lake) based on regression analysis. Consequently, these indexes cannot be applied to other study areas directly. When the MSWI and SWI are applied elsewhere, the corresponding coefficients of these indexes should be re-determined locally (Amani et al., 2018; Ghahremanloo et al., 2018). There are other uncertainties in the construction of MSWI, such as

water color, suspended sediments, shoal water area, and various pre-processing methods of SAR images that we will not detail in the current study.

5.3. Variations of water surface area and its eco-environmental impacts

Based on the standards outlined by Ramsar Convention, apart from the surrounding marshes, Ebinur Lake itself is a lake wetland (MacKay et al., 2009). The water and wetland resources played an irreplaceable role in XUAR. It is crucial to local environment and ecosystems to preserve wetlands, especially in inland arid regions (Zhao et al., 2013). Although the surface area of Ebinur lake in 2017 has reached an all-time high, it is important to pay more attention to the subsequent eco-environmental impacts. (Liu et al., 2002) has analyzed the effect of water level dynamics on the salinization of Ebinur Lake wetland. The water level of Ebinur Lake is 2.41 m in 2002, and the simultaneous salinized area reached 800 km². With the increasing lake water level, local soil salinity decreased slightly comparing to just a few years ago.

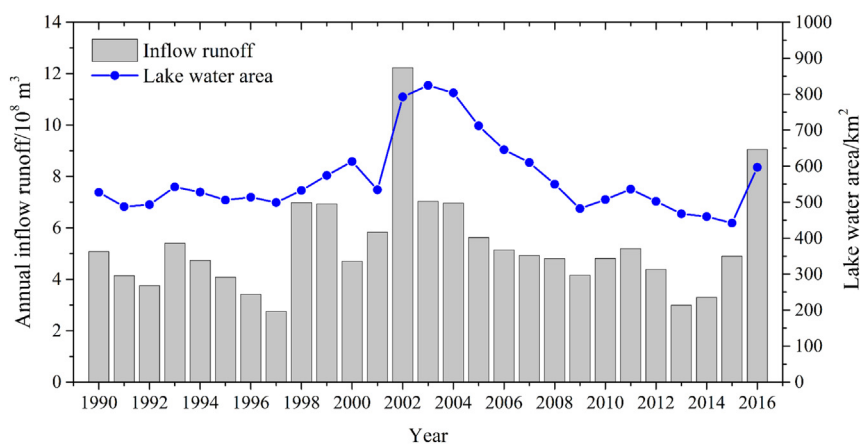


Fig. 9. The dynamic changes of surface area of Ebinur Lake and the volume of inflow water.

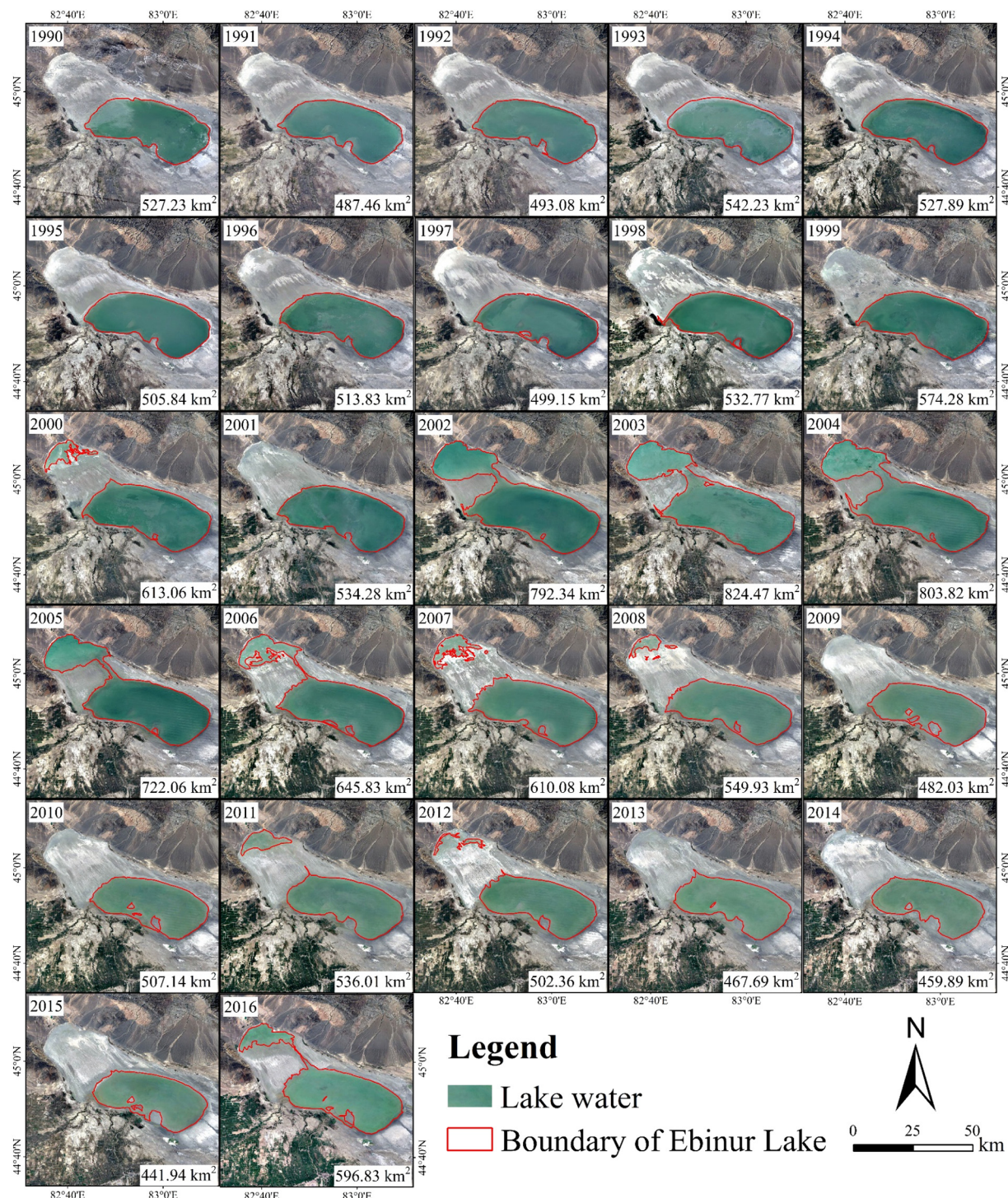


Fig. 10. Spatial and temporal dynamic changes of Ebinur Lake in Summer months from 1990 to 2016 (collected from <http://earthdata.nasa.gov/data/near-real-time-data-and-https://earthdata.nasa.gov/labs/worldview/>).

The distinct increase of precipitation in 2002 contributed greatly to more inflow runoff, and further led to the temporary expansion of lake area as well as higher groundwater level. In the study area, sand and sandy loam with strong capillary forces are the main soil types (Liu et al., 2011). The strong winds from the Alataw Pass could accelerate regional evaporation rate. Thereby, the shrunk of the lake might result in severe local soil salinization, and the bare playa serves as the source of salt-rich sand particles (Ma et al., 2014). The prevailing northwestern winds with salt-rich dusts could endanger the ecological environment in the Hexi Corridor Region and the entire North China Plain (Liu et al.,

2015).

Over the past decades, pesticide and fertilizer usage throughout the Ebinur Lake region is increasing, and the streamflow carried with massive untreated industrial wastewater and domestic sewage flows into the lake (Zhang et al., 2014). Because of the reduction of inflow water volume/level and resulting high-salinity lake water (about 112.4 g/L), the reoxygenation capacity of Ebinur Lake is impaired. Massive oxygen demanding materials and nutrients in the water makes the pollution in the study area more serious, and the lake water is now dominated by organic pollution (Wang et al., 2017b). Although the

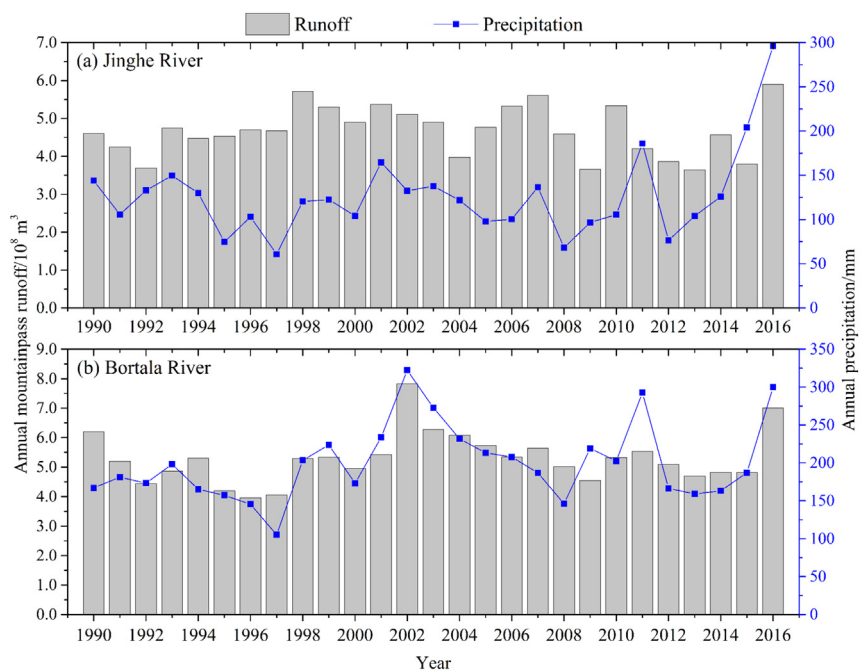


Fig. 11. The annual mountain-pass runoff and precipitation in Jinghe and Bortala River from 1990 to 2016.

Table 4
M-K trend test for annual runoff in Jinghe River and Bortala River.

Station	C.V.	Z	E_o	Trend
Jinghe River	0.14	4.59	0.43	increasing
Bortala River	0.20	-0.10	-0.01	slight descending

Note: C.V. means the coefficient of variation, Z means the standardized test statistics, E_o means the Sen slope estimator (change rate).

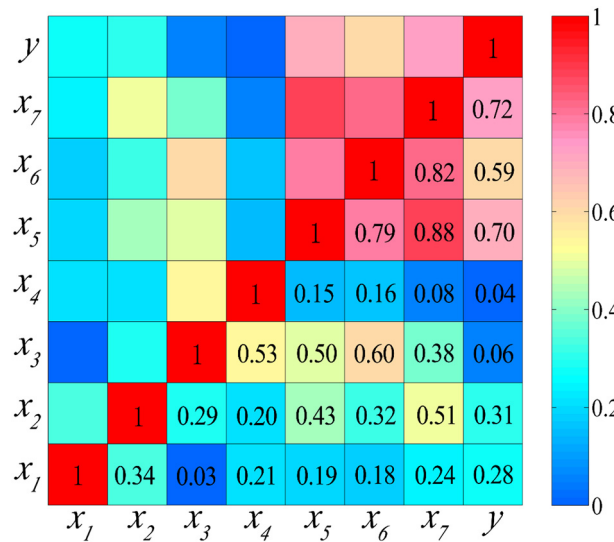


Fig. 12. Correlation between the annual mean temperature (x_1), mountain-pass annual runoff (x_2), mean precipitation (x_3) in Jinghe Station, annual mean temperature (x_4), annual mountain-pass runoff (x_5), mean precipitation (x_6) in Bole Station, inflow runoff volume (x_7), and surface area of Ebinur Lake (y) from 1990 to 2016.

water surface area is expanding, the current situation of surface water environment is still under threat. For this matter, to protect the fragile environment in the Ebinur Lake region, and design comprehensive eco-environment improvement plans, it is necessary to not only monitor the

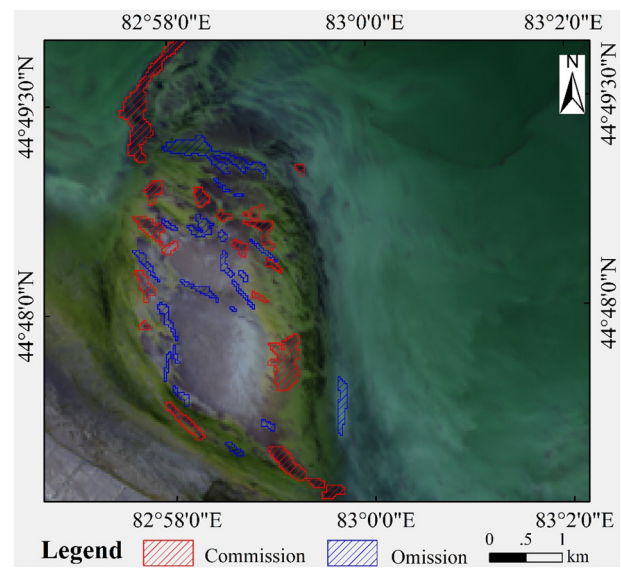


Fig. 13. The features in true color-Landsat-8 OLI (captured on July 27th, 2017) of the misclassification of water body extracted from MSWI scene.

change of water surface area, but also the change of water quality.

6. Conclusions

In this study, a modified Sentinel 1A water index (MSWI) is proposed based on the relationships between optical and SAR remote sensing imageries. Using the dynamic thresholds selected by Otsu method, the classification results are highly accurate with the optimal overall accuracy of 99.94% and kappa coefficient of 0.9971, respectively. The comparison of waterbody extraction between indexes of NDWI and MSWI suggests that it is reliable to use MSWI based on S1A data to extract the water surface areas in Ebinur Lake. For intra-annual scale, a time series analysis of surface areas of Ebinur Lake was conducted using S1A data from February 9th, 2017 to February 4th, 2018. The maximum lake surface area was 965.29 km² (April 22nd, 2017),

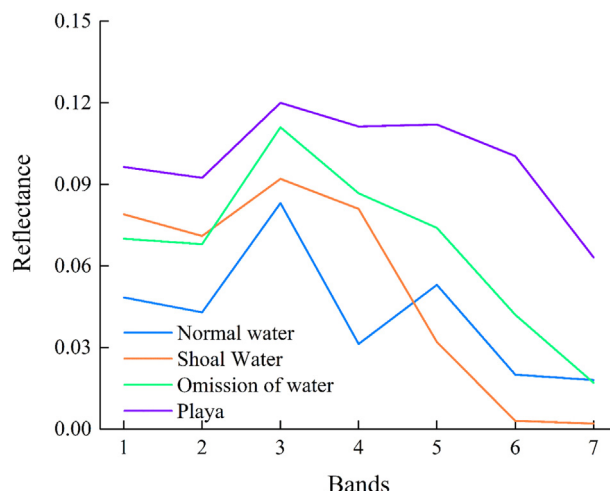


Fig. 14. The spectral reflectance of confusable zones in Landsat-8 OLI imagery captured on July 27th, 2017.

while the minimum value was 750.37 km² (September 1st, 2017), and the mean area was 831.51 km². The seasonal variations showed the stages of “sharp rising” – “significant decreasing” – “gradual stabilizing” in the study period. For inter-annual scale, the correlation between water surface area and inflow water volume was the highest (r -value = 0.72, $P < 0.001$), indicating that variations in the water surface area of Ebinur Lake are significantly correlated with the change of inflow. The newly constructed water index can be used for high-frequency (every 12-day) water body detection with high accuracy in the study area. The variations of Ebinur Lake's water surface area revealed by S1A data are crucial to evaluate how such variations impact on local eco-environment in the arid and semi-arid areas.

Acknowledgments

This study was supported by the National Natural Science Foundation of China (41771470, 41761041 and 31700386) and the Thousand Youth Talents Plan of China: Xinjiang Project. The funders had no role in study design, data collection and analysis, decision to publish, or preparation of the manuscript. The authors would like to thank Prof. Zhihui Liu, Dr. Maierdang Keyimu, and Dr. Abuduwaili Abulikemu for the support in providing data and linguistic assistance. We are especially grateful to the anonymous reviewers and editors for appraising our manuscript and for offering instructive comments.

References

- Ahmad, I., Tang, D., Wang, T., Wang, M., Wagan, B., 2015. Precipitation trends over time using Mann-Kendall and Spearman's rho tests in Swat River Basin, Pakistan. *Adv. Meteorol.* 2015, 15.
- Alesheikh, A.A., Ghorbanali, A., Nouri, N., 2007. Coastline change detection using remote sensing. *Int. J. Environ. Sci. Technol.* 4, 61–66.
- Amani, M., Salehi, B., Mahdavi, S., Granger, J., Brisco, B., 2017. Wetland classification in Newfoundland and Labrador using multi-source SAR and optical data integration. *GISci. Remote Sens.* 54, 779–796.
- Amani, M., Moshaveri, M.R., Mahdavi, S., 2018. Contemporary estimation of leaf area index and soil moisture using the red-NIR spectral space. *Remote Sens. Lett.* 9, 264–273.
- Bai, J., Chen, X., Li, J., Yang, L., Fang, H., 2011. Changes in the area of inland lakes in arid regions of central Asia during the past 30 years. *Environ. Monit. Assess.* 178, 247–256.
- Bao, A., et al., 2006. Estimation of the rational water area for controlling wind erosion in the dried-up basin of the Ebinur Lake and its effect detection. *Chin. Sci. Bull.* 51, 68–74.
- Beeton, A.M., 2002. Large freshwater lakes: present state, trends, and future. *Environ. Conserv.* 29, 21–38.
- Bennett, N.D., et al., 2013. Characterising performance of environmental models. *Environ. Model Softw.* 40, 1–20.
- Birkett, C.M., Mason, I.M., 1995. A new global lakes database for a remote sensing program studying climatically sensitive large lakes. *J. Great Lakes Res.* 21, 307–318.
- Brisco, B., Short, N., Sanden, J.V.D., Landry, R., Raymond, D., 2009. A semi-automated tool for surface water mapping with RADARSAT-1. *Can. J. Remote. Sens.* 35, 336–344.
- Brisco, B., Kapfer, M., Hirose, T., Tedford, B., Liu, J., 2011. Evaluation of C-band polarization diversity and polarimetry for wetland mapping. *Can. J. Remote. Sens.* 37, 82–92.
- Chai, T., Draxler, R.R., 2014. Root mean square error (RMSE) or mean absolute error (MAE)? – arguments against avoiding RMSE in the literature. *Geosci. Model Dev.* 7, 1247–1250.
- Dalponte, M., Örka, H.O., Ene, L.T., Gobakken, T., Næsset, E., 2014. Tree crown delineation and tree species classification in boreal forests using hyperspectral and ALS data. *Remote Sens. Environ.* 140, 306–317.
- Deng, Y., et al., 2017. Spatio-temporal change of lake water extent in Wuhan urban agglomeration based on Landsat images from 1987 to 2015. *Remote Sens.* 9, 270.
- Dong, J., Liao, M., Zhang, L., Gong, J., 2018. A unified approach of multitemporal SAR data filtering through adaptive estimation of complex covariance matrix. *IEEE Trans. Geosci. Remote Sens.* 56, 5320–5333.
- Eweys, O.A., et al., 2017. Disaggregation of SMOS soil moisture to 100 m resolution using MODIS optical/thermal and Sentinel-1 radar data: evaluation over a bare soil site in Morocco. *Remote Sens.* 9, 1155.
- Feng, L., et al., 2011. MODIS observations of the bottom topography and its inter-annual variability of Poyang Lake. *Remote Sens. Environ.* 115, 2729–2741.
- Feng, L., et al., 2012. Assessment of inundation changes of Poyang Lake using MODIS observations between 2000 and 2010. *Remote Sens. Environ.* 121, 80–92.
- Ge, Y., Abuduwaili, J., Ma, L., Wu, N., Liu, D., 2016. Potential transport pathways of dust emanating from the playa of Ebinur Lake, Xinjiang, in arid northwest China. *Atmos. Res.* 178–179, 196–206.
- George, G., Hurley, M., Hewitt, D., 2007. The impact of climate change on the physical characteristics of the larger lakes in the English Lake District. *Freshw. Biol.* 52, 1647–1666.
- Geudtner, D., Torres, R., Snoeijs, P., Davidson, M., Rommen, B., 2014. In: *Sentinel-1 System Capabilities and Applications*. 2014 IEEE Geoscience and Remote Sensing Symposium. pp. 1457–1460.
- Ghahremanloo, M., Moshaveri, M.R., Amani, M., 2018. Soil moisture estimation using land surface temperature and soil temperature at 5 cm depth. *Int. J. Remote Sens.* 1–14.
- Gong, P., et al., 2013. Finer resolution observation and monitoring of global land cover: first mapping results with Landsat TM and ETM+ data. *Int. J. Remote Sens.* 34, 2607–2654.
- Haas, E.M., Bartholomé, E., Lambin, E.F., Vanacker, V., 2011. Remotely sensed surface water extent as an indicator of short-term changes in ecohydrological processes in sub-Saharan Western Africa. *Remote Sens. Environ.* 115, 3436–3445.
- He, X., et al., 2015. Effects of simulated nitrogen deposition on soil respiration in a *Populus euphratica* community in the Ebinur Lake Area, a desert ecosystem of Northwestern China. *PLoS One* 10, e0137827.
- Holmgren, M., et al., 2006. Extreme climatic events shape arid and semiarid ecosystems. *Front. Ecol. Environ.* 4, 87–95.
- Horritt, M.S., Mason, D.C., Luckman, A.J., 2001. Flood boundary delineation from synthetic aperture radar imagery using a statistical active contour model. *Int. J. Remote Sens.* 22, 2489–2507.
- Jin, H., Mountrakis, G., Stehman, S.V., 2014. Assessing integration of intensity, polarimetric scattering, interferometric coherence and spatial texture metrics in PALSAR-derived land cover classification. *ISPRS J. Photogramm. Remote Sens.* 98, 70–84.
- Jing, Y., Zhang, F., Wang, X., 2018. Monitoring dynamics and driving forces of lake changes in different seasons in Xinjiang using multi-source remote sensing. *Eur. J. Remote Sens.* 51, 150–165.
- Kendall, M.G., 1975. *Rank Correlation Methods*, 4th ed. Charles Griffin, London.
- Kisi, O., Ay, M., 2014. Comparison of Mann-Kendall and innovative trend method for water quality parameters of the Kizilirmak River, Turkey. *J. Hydrol.* 513, 362–375.
- Kyriou, A., Nikolakopoulos, K., 2015. Flood Mapping from Sentinel-1 and Landsat-8 Data: A Case Study from River Evros, Greece, SPIE Remote Sensing, SPIE, pp. 10.
- Lacaux, J.P., Tourre, Y.M., Vignolles, C., Ndione, J.A., Lafaye, M., 2007. Classification of ponds from high-spatial resolution remote sensing: application to Rift Valley fever epidemics in Senegal. *Remote Sens. Environ.* 106, 66–74.
- LeBlanc, L.A., Kuivila, K.M., 2008. Occurrence, distribution and transport of pesticides into the Salton Sea Basin, California, 2001–2002. *Hydrobiologia* 604, 151–172.
- Li, X.Y., Ma, Y.J., Xu, H.Y., Wang, J.H., Zhang, D.S., 2009. Impact of land use and land cover change on environmental degradation in lake Qinghai watershed, northeast Qinghai-Tibet Plateau. *Land Degrad. Dev.* 20, 69–83.
- Li, Q., et al., 2015. MODIS-derived spatiotemporal changes of Major Lake surface areas in arid Xinjiang, China, 2000–2014. *Water* 7, 5731–5751.
- Li, Z., et al., 2017. Landsat 15-m panchromatic-assisted downscaling (LPAD) of the 30-m reflective wavelength bands to Sentinel-2 20-m resolution. *Remote Sens.* 9, 755.
- Liao, A., et al., 2014. High-resolution remote sensing mapping of global land water. *Sci. China Earth Sci.* 57, 2305–2316.
- Lillesand, T., Kiefer, R.W., Chipman, J., 1994. *Remote Sensing and Image Interpretation*. John Wiley & Sons, New York.
- Liu, Y., Wang, X., Wu, Y., 2002. Research on the water level change effect on the salinity of everglade around Ebinur Lake. *J. Arid Land Resour. Environ.* 24, 108–111 (in Chinese).
- Liu, J., Liu, M., Zhuang, D., Zhang, Z., Deng, X., 2003. Study on spatial pattern of land-use change in China during 1995–2000. *Sci. China Ser. D Earth Sci.* 46, 373–384.
- Liu, D., Abuduwaili, J., Lei, J., Wu, G., 2011. Deposition rate and chemical composition of the Aeolian dust from a bare saline playa, Ebinur Lake, Xinjiang, China. *Water Air Soil Pollut.* 218, 175–184.
- Liu, D., Abuduwaili, J., Wang, L., 2015. Salt dust storm in the Ebinur Lake region: its 50-

- year dynamic changes and response to climate changes and human activities. *Nat. Hazards* 77, 1069–1080.
- Ma, M., Wang, X., Veroustraete, F., Dong, L., 2007. Change in area of Ebinur Lake during the 1998–2005 period. *Int. J. Remote Sens.* 28, 5523–5533.
- Ma, R., et al., 2010. A half-century of changes in China's lakes: global warming or human influence? *Geophys. Res. Lett.* 37, L24106.
- Ma, L., Wu, J., Liu, W., Abuduwaili, J., 2014. Distinguishing between anthropogenic and climatic impacts on lake size: a modeling approach using data from Ebinur Lake in arid northwest China. *J. Limnol.* 73, 148–155.
- MacKay, H., et al., 2009. The role of earth observation (EO) technologies in supporting implementation of the Ramsar Convention on Wetlands. *J. Environ. Manag.* 90, 2234–2242.
- Mahdavi, S., et al., 2017. Object-based classification of wetlands in Newfoundland and Labrador using multi-temporal PolSAR data. *Can. J. Remote. Sens.* 43, 432–450.
- Malenovský, Z., et al., 2012. Sentinels for science: potential of Sentinel-1, -2, and -3 missions for scientific observations of ocean, cryosphere, and land. *Remote Sens. Environ.* 120, 91–101.
- Mann, H.B., 1945. Nonparametric tests against trend. *Econometrica* 13, 245–259.
- Mason, D.C., Schumann, G.J.P., Neal, J.C., García-Pintado, J., Bates, P.D., 2012. Automatic near real-time selection of flood water levels from high resolution synthetic aperture radar images for assimilation into hydraulic models: a case study. *Remote Sens. Environ.* 124, 705–716.
- McFeeters, S.K., 1996. The use of the normalized difference water index (NDWI) in the delineation of open water features. *Int. J. Remote Sens.* 17, 1425–1432.
- O'Reilly, C.M., et al., 2015. Rapid and highly variable warming of lake surface waters around the globe. *Geophys. Res. Lett.* 42, 10,773–10,781.
- Otsu, N., 1979. A threshold selection method from gray-level histograms. *IEEE Trans. Syst. Man Cybern.* 9, 62–69.
- Passaro, M., Müller, F.L., Dettmering, D., 2018. Lead detection using Cryosat-2 delay-doppler processing and Sentinel-1 SAR images. *Adv. Space Res.* 62, 1610–1625.
- Plank, S., 2014. Rapid damage assessment by means of multi-temporal SAR — a comprehensive review and outlook to Sentinel-1. *Remote Sens.* 6, 4870.
- Ridd, M.K., Liu, J., 1998. A comparison of four algorithms for change detection in an urban environment. *Remote Sens. Environ.* 63, 95–100.
- Rosser, J.F., Leibovici, D.G., Jackson, M.J., 2017. Rapid flood inundation mapping using social media, remote sensing and topographic data. *Nat. Hazards* 87, 103–120.
- Roy, D.P., et al., 2014. Landsat-8: science and product vision for terrestrial global change research. *Remote Sens. Environ.* 145, 154–172.
- Shao, Y., et al., 2012. SAR data for subsurface saline lacustrine deposits detection and primary interpretation on the evolution of the vanished Lop Nur Lake. *Can. J. Remote. Sens.* 38, 267–280.
- Sharma, R., Tateishi, R., Hara, K., Nguyen, L., 2015. Developing superfine water index (SWI) for global water cover mapping using MODIS data. *Remote Sens.* 7, 13807–13841.
- Silveira, M., Heleno, S., 2009. Separation between water and land in SAR images using region-based level sets. *IEEE Geosci. Remote Sens. Lett.* 6, 471–475.
- Singh, A., Seitz, F., Schwatke, C., 2012. Inter-annual water storage changes in the Aral Sea from multi-mission satellite altimetry, optical remote sensing, and GRACE satellite gravimetry. *Remote Sens. Environ.* 123, 187–195.
- Stanev, E.V., Peneva, E.L., Mercier, F., 2004. Temporal and spatial patterns of sea level in inland basins: recent events in the Aral Sea. *Geophys. Res. Lett.* 31, L15505.
- Stephanie, L., Temilola, E.F., Frederick, P., 2014. Flood extent mapping for Namibia using change detection and thresholding with SAR. *Environ. Res. Lett.* 9, 035002.
- Su, X., Liu, Z., Wei, T., Wang, Y., Liu, Y., 2016. Change of Ebinur Lake area and its response characteristics of the runoff change. *Research of Soil and Water Conservation* 23, 252–256 (in Chinese).
- Tian, H., et al., 2017. Dynamic monitoring of the largest freshwater Lake in China using a new water index derived from high spatiotemporal resolution Sentinel-1A data. *Remote Sens.* 9, 521.
- Tian, H., Wu, M., Wang, L., Niu, Z., 2018. Mapping early, middle and late Rice extent using sentinel-1A and Landsat-8 data in the Poyang Lake plain, China. *Sensors* 18, 185.
- Torres, R., et al., 2012. GMES Sentinel-1 mission. *Remote Sens. Environ.* 120, 9–24.
- Veloso, A., et al., 2017. Understanding the temporal behavior of crops using Sentinel-1 and Sentinel-2-like data for agricultural applications. *Remote Sens. Environ.* 199, 415–426.
- Wang, S., et al., 2015. A simple enhanced water index (EWI) for percent surface water estimation using Landsat data. *IEEE J. Sel. Top. Appl. Earth Obs. Remote Sens.* 8, 90–97.
- Wang, J., et al., 2017a. Desert soil clay content estimation using reflectance spectroscopy preprocessed by fractional derivative. *PLoS One* 12, e0184836.
- Wang, X., et al., 2017b. Evaluation and estimation of surface water quality in an arid region based on EEM-PARAFAC and 3D fluorescence spectral index: a case study of the Ebinur Lake Watershed, China. *CATENA* 155, 62–74.
- Wang, J., Ding, J., Abulimiti, A., Cai, L., 2018a. Quantitative estimation of soil salinity by means of different modeling methods and visible-near infrared (VIS-NIR) spectroscopy, Ebinur Lake Wetland, Northwest China. *PeerJ* 6, e4703.
- Wang, Y., Liu, Z., Yao, J., Bayin, C., Zhu, Y., 2018b. Hydrological response of runoff to climate change of typical tributaries in Ebinur Lake Basin of Xinjiang. *Water Resour. 45*, 160–168.
- Williamson, C.E., Saros, J.E., Vincent, W.F., Smol, J.P., 2009. Lakes and reservoirs as sentinels, integrators, and regulators of climate change. *Limnol. Oceanogr.* 54, 2273–2282.
- Xu, H., 2006. Modification of normalised difference water index (NDWI) to enhance open water features in remotely sensed imagery. *Int. J. Remote Sens.* 27, 3025–3033.
- Yang, X., Lu, X., 2014. Drastic change in China's lakes and reservoirs over the past decades. *Sci. Rep.* 4, 6041.
- Zeng, L., Schmitt, M., Li, L., Zhu, X.X., 2017. Analysing changes of the Poyang Lake water area using Sentinel-1 synthetic aperture radar imagery. *Int. J. Remote Sens.* 38, 7041–7069.
- Zhang, F., et al., 2014. The influence of natural and human factors in the shrinking of the Ebinur Lake, Xinjiang, China, during the 1972–2013 period. *Environ. Monit. Assess.* 187, 4128.
- Zhang, F., et al., 2015. The spatial and temporal dynamic changes and driving forces in the surface area of ebinur lake from 1998–2013. *Acta Ecol. Sin.* 35, 2848–2859 (in Chinese).
- Zhao, R., et al., 2013. Land use and land cover change and driving mechanism in the arid inland river basin: a case study of Tarim River, Xinjiang, China. *Environ. Earth Sci.* 68, 591–604.
- Zhao, Y., Liu, J., Zhang, B., Hong, W., Wu, Y., 2015. Adaptive total variation regularization based SAR image despeckling and despeckling evaluation index. *IEEE Trans. Geosci. Remote Sens.* 53, 2765–2774.
- Zhuang, H., Fan, H., Deng, K., Yao, G., 2018. A spatial-temporal adaptive neighborhood-based ratio approach for change detection in SAR images. *Remote Sens.* 10, 1295.